

Letter

Real-time propagator eigenstates

F Oppermann , N Eicke and M Lein* 

Institute of Theoretical Physics, Leibniz University Hannover, Appelstraße 2, 30167 Hannover, Germany

E-mail: lein@itp.uni-hannover.de

Received 21 June 2022, revised 18 August 2022

Accepted for publication 21 August 2022

Published 2 September 2022



CrossMark

Abstract

Obtaining a numerical solution of the time-dependent Schrödinger equation requires an initial state for the time evolution. If the system Hamiltonian can be split into a time-independent part and a time-dependent perturbation, the initial state is typically chosen as an eigenstate of the former. For propagation using approximate methods such as operator splitting, we show that both imaginary-time evolution and diagonalization of the time-independent Hamiltonian produce states that are not exactly stationary in absence of the perturbation. In order to avoid artifacts from these non-stationary initial states, we propose an iterative method for calculating eigenstates of the real-time propagator. We compare the performance of different initial states by simulating ionization of a model atom in a short laser pulse and we demonstrate that much lower noise levels can be achieved with the real-time propagator eigenstates.

Keywords: time-independent Schrödinger equation, time-dependent Schrödinger equation, eigenstates, split-operator method, laser-induced ionization


(Some figures may appear in colour only in the online journal)

1. Introduction

In many fields of theoretical quantum physics it is necessary to calculate eigenstates of operators. Energy eigenstates of a quantum system, i.e. eigenstates of a time-independent Hamiltonian H_0 , are of particular relevance because they are stationary when they evolve in real time according to the time-dependent Schrödinger equation (TDSE) with the Hamiltonian H_0 . Here, ‘stationary’ means that the state changes only by a purely time-dependent phase factor. A standard situation in quantum physics is that a system starts out in an energy eigenstate and then interacts with external fields described by a time-dependent interaction Hamiltonian $H_i(t)$ so that the TDSE for the real-time propagation (RTP) reads

$$i \frac{d}{dt} |\psi(t)\rangle = H(t) |\psi(t)\rangle \quad (1)$$

* Author to whom any correspondence should be addressed.

 Original content from this work may be used under the terms of the [Creative Commons Attribution 4.0 licence](https://creativecommons.org/licenses/by/4.0/). Any further distribution of this work must maintain attribution to the author(s) and the title of the work, journal citation and DOI.

(atomic units are used unless stated otherwise) with the total Hamiltonian $H(t) = H_0 + H_i(t)$. If the external fields are of moderate strength, the deviation of the time-dependent state $|\psi(t)\rangle$ from the initial state might be small but nevertheless too large to be conveniently described by time-dependent perturbation theory. In this case, the numerical solution of the TDSE is a commonly used approach. However, the accuracy of any numerical method is limited, so that eigenstates of H_0 or their numerical implementations are not necessarily stationary under numerical propagation even if $H_i = 0$. If these errors are comparable with the physical excitations caused by the external fields, the actual physics will be obscured and the numerical results will not be reliable. In this letter, we show that the problem is elegantly circumvented by choosing the initial state as an eigenstate of the numerical real-time propagator of the field-free system rather than an eigenstate of the field-free Hamiltonian.

A simple, long-standing and popular method for obtaining ground states is imaginary-time propagation (ITP), also known as relaxation method, i.e. the repeated application of the numerical short-time propagator with an imaginary time step starting from an arbitrary initial state [1]. It has been applied

not only to local potentials of one-particle and few-particle systems [2], but also to obtain many-electron Kohn–Sham ground states in density functional theory [3, 4], and to find solutions of the Gross–Pitaevskii equation [5, 6]. The method works due to the relative suppression of excited states by factors that are exponential in the energy differences relative to the ground state. When using the state resulting from ITP as an initial state for RTP, we face the same problem as described above: the state might not be exactly stationary under numerical RTP.

This letter focuses on the split-operator method [7, 8] as a propagation method, which is similarly widespread as ITP [2, 4, 9]. In principle, our proposal of using real-time propagator eigenstates (RTPEs) can be applied to any RTP method, but our study is less relevant for propagation schemes where the error term in the propagators does not change the eigenstates, e.g. Crank–Nicolson propagation [10] or the Chebychev method [11].

In what follows, we first describe briefly why numerical ITP and numerical RTP have different eigenstates and how to calculate eigenstates for a general operator using the *power method*. We then apply this method to compare imaginary-time propagator eigenstates (ITPEs) to RTPEs in a simple one-dimensional atom. We evaluate the performance of these states when used as initial states in real-time simulations of ionization of the model atom by short laser pulses. The results show that simulations with RTPEs are reliable in situations involving low photoelectron yields, where other initial states fail to produce physical results.

2. Numerical approximations and power method

Parts of this section have been presented before [12]. In the split-operator scheme [7, 8], the short-time propagator for a Hamiltonian $H_0 = T + V$ with a momentum-dependent part T and a position-dependent part V is approximated as

$$U_{\text{RTP}}^{\text{SO}} := e^{-iV\Delta t/2} e^{-iT\Delta t} e^{-iV\Delta t/2} = e^{-iH_{\text{eff}}\Delta t}. \quad (2)$$

This operator splitting is not exact since

$$H_{\text{eff}} = H_0 + \frac{\Delta t^2}{24}[V + 2T, [V, T]] + \mathcal{O}(\Delta t^4). \quad (3)$$

Hence, $U_{\text{RTP}}^{\text{SO}}$ is actually the short-time propagator for a *different* Hamiltonian H_{eff} . The exact short-time propagator for H_0 is

$$U_{\text{RTP}} = e^{-iH_0\Delta t} = U_{\text{RTP}}^{\text{SO}} + \frac{i\Delta t^3}{24}[V + 2T, [V, T]] + \mathcal{O}(\Delta t^4). \quad (4)$$

The similarity of the error terms in (3) and (4) is analogous to time-dependent perturbation theory, where the lowest-order change of the short-time propagator is proportional to the change of the Hamiltonian. Because these error terms are not functionals of H_0 , it is obvious that U_{RTP} and $U_{\text{RTP}}^{\text{SO}}$ have not exactly the same eigenstates. Moreover, when inserting an imaginary time step $\Delta t = -i\Delta\tau$ instead of a real time step into the split-operator propagator, the error term in (3) switches

sign. Hence, the eigenstates of the imaginary-time propagator

$$U_{\text{ITP}}^{\text{SO}} = e^{-V\Delta\tau/2} e^{-T\Delta\tau} e^{-V\Delta\tau/2} \quad (5)$$

also differ from those of $U_{\text{RTP}}^{\text{SO}}$, no matter how large or small the step size $\Delta\tau$ is chosen. Therefore, to obtain states that are numerically stationary under RTP, we need to find the eigenstates of $U_{\text{RTP}}^{\text{SO}}$.

Even when it is not feasible to diagonalize an operator exactly, it is often possible to find eigenstates by iterative methods. ITP is an example of this: it finds an eigenstate of $U_{\text{ITP}}^{\text{SO}}$. More generally, let A be an operator whose normalized eigenstates $|\chi_n\rangle$ satisfy

$$A|\chi_n\rangle = \alpha_n|\chi_n\rangle. \quad (6)$$

and form a basis. For an arbitrary state $|\psi_0\rangle = \sum_n c_n|\chi_n\rangle$ define

$$|\psi_{k+1}\rangle = \frac{A|\psi_k\rangle}{\|A|\psi_k\rangle\|}, \quad k = 1, 2, 3, \dots \quad (7)$$

This sequence converges to the eigenstate corresponding to the eigenvalue with the largest magnitude that is present in $|\psi_0\rangle$. More precisely, if $|\alpha_0| > |\alpha_n| \forall n \neq 0$ and $c_0 \neq 0$, then $|\psi_k\rangle \rightarrow |\chi_0\rangle$ for $k \rightarrow \infty$ (up to a phase factor) [13]. These very basic considerations lead to the probably simplest eigenstate calculation scheme, known as the power method: apply some power A^j of the operator A , normalize, and repeat until changes are sufficiently small. Eigenstates other than $|\chi_0\rangle$ can be calculated with the same method when additionally projecting out (i.e. removing) all states with larger eigenvalues once they are known. In numerical implementations the projection has to be done repeatedly because numerical errors can cause the unwanted states to reappear in the course of the iteration.

To use the power method to search for eigenvalues other than those with large absolute values, one may transform the spectrum of an operator. ITP is an example for this: instead of H_0 , the operator $A = e^{-H_0\Delta\tau}$ (or an approximate implementation of it, such as the split-operator imaginary-time propagator (5)) is considered and thus the ground-state energy of H_0 is transformed into the largest eigenvalue of A .

For calculating RTPEs—eigenstates of the unitary real-time propagator—it is necessary to transform the spectrum to make the power method converge at all, since all eigenvalues $e^{-iE_k\Delta t}$ have magnitude 1. (For the approximate propagator, the ‘energies’ E_k in this expression are not necessarily equal to, but very close to the eigenvalues of the Hamiltonian. Strictly speaking, in the following discussion, the term energy refers to the real-time propagator.) A simple shift in the complex plane solves this issue,

$$A = U_{\text{RTP}}^{\text{SO}} + \lambda, \quad \lambda \in \mathbb{C}, \quad (8)$$

see figure 1 for examples. Hence, in our implementation, the eigenstates are found by repeated application of the operator (8) and normalization of the state. The shift λ does not change the eigenstates but only the eigenvalues. It is only added for the eigenstate calculation, not in the actual time evolution. The optimal shift depends on the structure of the

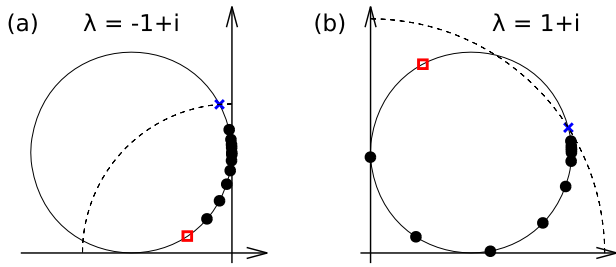


Figure 1. Illustration of the spectrum (symbols on the circles) of the shifted real-time propagator in the complex plane. The horizontal (vertical) axis shows the real (imaginary) part of the eigenvalues. The ground-state eigenvalue (blue cross) and the value corresponding to the maximum energy E_{\max} (red square) are highlighted. (a) The shift $\lambda = -1 + i$ is applicable if $E_{\max} \Delta t < \pi/2$. It facilitates fast convergence. (b) The shift $\lambda = 1 + i$ allows for larger values $E_{\max} \Delta t < 3\pi/2$. In both (a) and (b), the ground-state eigenvalue is guaranteed to have the largest magnitude (indicated by the dashed circle) if $|E_0 \Delta t| \ll \pi/2$.

spectrum. We assume that the desired ground-state energy E_0 is negative (which can always be achieved by shifting the potential or, equivalently, by multiplying $U_{\text{RTP}}^{\text{SO}}$ with a suitable phase factor). In finite-dimensional implementations there is also a largest energy E_{\max} . The split-operator method is typically used together with the discrete Fourier transform on an equidistant grid with spacing Δx to represent the momentum-dependent operators as multiplications in Fourier space. In this case, $T = -\frac{1}{2} d^2/dx^2$ implies $E_{\max} \approx p_{\max}^2/2$ with $p_{\max} = \pi/\Delta x$. To avoid overlapping eigenvalues on the unit circle, Δt must be chosen such that

$$(E_{\max} - E_0)\Delta t < 2\pi. \quad (9)$$

The method works if and only if the shift λ is chosen such that the ground state corresponds to the eigenvalue of A with the largest magnitude. Figure 1 illustrates this by showing the locations of the eigenvalues in the complex plane. Figure 1(a) shows $\lambda = -1 + i$, which certainly works if $|E_0 \Delta t| \ll \pi/2$ and $E_{\max} \Delta t < \pi/2$. If $|E_0 \Delta t| \ll \pi/2$ and $E_{\max} \Delta t < 3\pi/2$ (i.e. allowing larger time steps), the shift $\lambda = 1 + i$ is a safe default, see figure 1(b). RTPEs in this letter are calculated with $\lambda = 1 + i$. The convergence speed depends on the ratio of the two largest eigenvalues, typically those corresponding to the ground state and the first excited bound state with energy E_1 . If $|E_0 \Delta t| \ll \pi/2$, the difference between these eigenvalues is imaginary in first order, $e^{-iE_0 \Delta t} - e^{-iE_1 \Delta t} \approx i(E_1 - E_0)\Delta t + \mathcal{O}(\Delta t^2)$. Thus, shifting these eigenvalues to the imaginary axis by choosing $\text{Re } \lambda = -1$ maximizes the ratio in magnitude.

The step size $\Delta \tau$ in ITP is in principle arbitrary. A typical procedure is to start with a large time step size for quick and rough convergence, followed by reduced step sizes in order to reduce errors in the split-operator approximation. In contrast, Δt is fixed at the same value that is used in the actual time propagation and due to the constraints described above it is not possible to increase its value arbitrarily for increased convergence speed. On the one hand this reduces flexibility and fine-tuning of the convergence speed. On the other hand it

takes away the burden of an additional non-physical parameter that has to be controlled separately. In practice, it can be convenient to begin with ITP for fast convergence and then switch to the power method for the shifted real-time propagator for finding the RTPEs.

The power method can also be used to calculate eigenstates of H_0 , e.g. by using the shifted operator $A = H_0 - E_{\max}$ so that all eigenvalues are negative and the ground-state eigenvalue has the largest magnitude. From (3) one could assume that eigenstates of H_0 are ‘halfway’ between ITPEs and RTPEs if $\Delta \tau = \Delta t$. In practice, however, H_0 eigenstates and ITPEs are similarly unstable, so the former are no significant improvement over the latter.

3. Example system

As an example application, we consider a one-dimensional model hydrogen atom in a linearly polarized laser pulse. The potential is given by $V(x) = -1/\sqrt{x^2 + a}$ with $a = 2$ a.u. The Hamiltonian in velocity gauge is $H(t) = (p + A(t))^2/2 + V(x)$. For this specific value of a , the field-free system ($A(t) = 0$) has an analytic ground-state solution with energy $E_0 = -0.5$ a.u. [14]. Numerically, both the potential and the position wave function are represented on an equidistant grid with grid spacing $\Delta x = 0.2$ a.u. For the simulation with external field, enough grid points (typically 8192) are used so that the wave function does not come close to the grid boundary during the time evolution. The momentum part in the split-operator scheme is implemented using fast Fourier transforms.

Figure 2 shows the ground state of the field-free system, calculated by various methods. When using the power method we find that after 10^5 steps, the ITPE seems to be far superior to the RTPe which has a high-lying tail at 10^{-17} whereas the ITPE is already at the noise level of around 10^{-30} . This result demonstrates the fast convergence of the ITP method. Another 10^5 steps later, however, the RTPe shows no qualitative difference to the ITPE anymore.

Both the real-time and the imaginary-time propagators as well as the Hamiltonian can also be diagonalized directly for this one-dimensional system. To this end, the matrix representation in position space is calculated, e.g.

$$(U_{\text{RTP}}^{\text{SO}})_{jk} = \langle x_j | U_{\text{RTP}}^{\text{SO}} | x_k \rangle, \quad (10)$$

where $|x_j\rangle$ is a position wave function that is non-vanishing only at grid point j . This matrix is unitary (for $U_{\text{RTP}}^{\text{SO}}$) or Hermitian (for $U_{\text{ITP}}^{\text{SO}}$ or H_0) and can be diagonalized. Diagonalization does not provide lower noise levels or significantly better results than 2×10^5 steps of the power method, indicating good convergence of the power method, see figure 2. Although the converged states do not show qualitative differences on the scale of figure 2, they will show important differences when used in the time-dependent calculations.

The laser pulse in the time-dependent Hamiltonian operator is defined by its vector potential $A(t) = A_0 \sin^2(\pi t/T_p) \cos(\omega(t - T_p/2))$, where T_p is the total pulse duration and $0 \leq t \leq T_p$. Here, $T_p = 10 \times 2\pi/\omega$ (ten-cycle pulse) and ω corresponds to 450 nm wavelength ($\omega \approx 0.101$ a.u.).

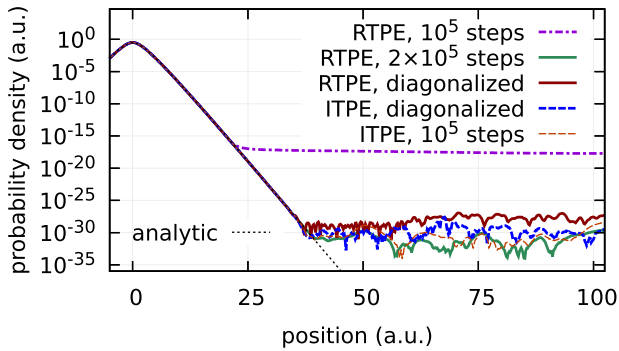


Figure 2. Position-space probability distributions of ground states calculated on 1024 grid points with a grid spacing of 0.2 a.u. The RTPEs (dot-dashed and solid lines) correspond to a time step of 0.02 a.u., the ITPEs (dashed lines) are calculated with $\Delta\tau = 0.02$ a.u. As the system is symmetric, we show only the right half of the grid completely. It can be seen that 10^5 steps of the ITP are much more effective in suppressing the ‘tail’ of the wave function than the same number of steps of the RTP. After twice the time, however, there is no qualitative difference visible between the propagators. Note that diagonalizing the RTP or ITP does not push the noise level further down. The analytic ground state (black dotted line) falls exponentially.

Our observables in this benchmark system are the ionization yield which we define as the probability to find the electron in $|x| > R_0 := 30$ a.u.,

$$\int_{|x|>R_0} |\langle x|\psi(T_p)\rangle|^2 dx. \quad (11)$$

and the photoelectron energy spectrum which we calculate by projecting the final wave function onto unbound eigenstates $|\psi_E\rangle$ that are calculated by diagonalizing the real-time propagator.

4. Results and discussion

The parameters of our time-dependent system are such that we expect ionization to be in the multiphoton regime (Keldysh parameter $\sqrt{2I_p}/A_0 > 1$, where $I_p = -E_0$ is the ionization potential). Therefore, the ionization yield is expected to increase with the laser intensity I approximately as a power law I^N where N is the number of photons needed to overcome the ionization threshold. The model system can be ionized by absorption of five 450 nm photons, i.e. the ionization yield for this process scales like I^5 . Indeed, for high intensities above 10^{12} W cm⁻², figure 3 shows this behaviour, irrespective of the chosen calculation method for the ground state. However, decreasing the intensity shows the background noise in the ITPE quickly. Even at vanishing intensity the ‘ionization probability’ is $>10^{-12}$ for the chosen time-step sizes. In the limit of small imaginary time steps $\Delta\tau$, ITPEs approach H_0 eigenstates which do not provide better performance (black solid curve). The noise level can be lowered slightly by decreasing the real-time step size Δt for the propagation in the laser field (thus decreasing the error terms in (3) and (4)) but at the cost of increased computation time (red dashed curve).

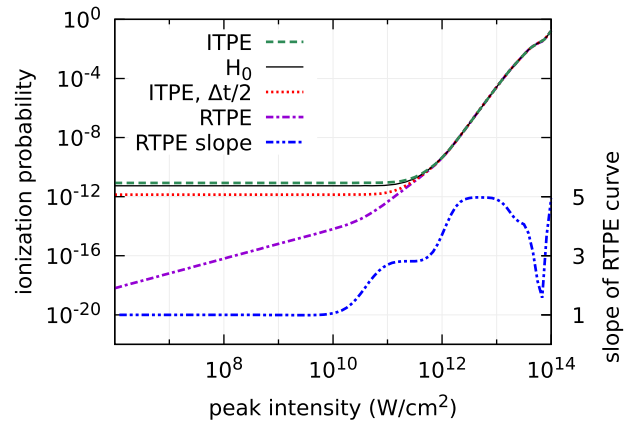


Figure 3. Ionization yield as a function of laser peak intensity for different initial states. For small intensities, the calculations starting with ITPEs or H_0 eigenstates approach relatively large ($>10^{-12}$) unphysical values which completely conceal the physical process that is visible with RTPEs: one-photon ionization due to photons from the high-frequency tail of the laser spectrum. The ITPE (state used for the dashed curves) is calculated by diagonalizing the ITP operator with $\Delta\tau = 0.01$ a.u. The H_0 eigenstate (state used for the thin black solid line) is calculated by diagonalizing the Hamiltonian. The RTPE (state used for the dot-dashed curve with squares) is calculated by 2×10^5 iterations of the power method with $\Delta t = 0.02$ a.u. Propagation in the laser field is carried out with $\Delta t = 0.02$ a.u., except for the red dashed curve with $\Delta t = 0.01$ a.u. Additionally the intensity-dependent slope of the RTPE ionization yield is shown to highlight the transition from one-photon over three-photon to five-photon ionization.

In contrast, the RTPE ionization yield continues to fall by many orders of magnitude with decreasing intensity. The field-free limit (i.e. propagation for the duration of the laser pulse but with $A_0 = 0$) is 4×10^{-24} . It is almost identical to the ‘ionization yield’ of the initial state prior to time evolution according to the definition (11). At low intensities, we observe that the dependence of the yield on intensity is flatter than I^5 . In figure 3 we include a curve showing the intensity-dependent slope of the yield and we find that the slope decreases from 5 through 3 to 1 as we decrease the intensity. This happens because the finite length of the laser pulse implies that the frequency spectrum of the pulse covers a broad range of frequencies. The highest frequencies are able to ionize the atom with just one photon. Therefore, at small intensities single-photon ionization from the high-frequency tail of the spectrum dominates the ionization signal.

As a second observable, figure 4 shows the energy spectrum of the photoelectron at the end of the laser pulse for different peak intensities and initial states. In multicycle non-resonant above-threshold ionization (ATI) with linearly polarized fields, the photoelectron spectrum exhibits peaks at the energies

$$E_{el,n} = n\omega - I_p - U_p, \quad (12)$$

where n counts the number of absorbed photons and $U_p = A_0^2/4$ is the ponderomotive potential [15]. The high-intensity curves in figure 4 show clear ATI peaks at the expected positions. Here, the RTPE initial state produces a clean ATI peak structure over the entire range of displayed photoelectron energies, while the ITPE initial state is able to reproduce the

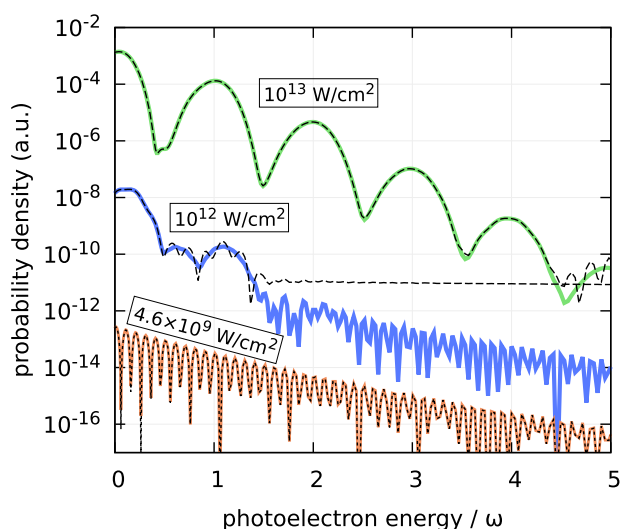


Figure 4. Photoelectron energy spectrum after ionization with a ten-cycle 450 nm laser pulse at three different peak intensities. Solid coloured lines show results of RTPE calculations; they give sensible spectra for all intensities. Black dashed lines are calculated using the ITPE as initial state. At $10^{13} \text{ W cm}^{-2}$ intensity, RTPE and ITPE agree perfectly for the first five peaks, whereas at $10^{12} \text{ W cm}^{-2}$ intensity already the second ATI peak shows unphysical oscillations. At small intensities, the photoelectron spectrum is dominated by one-photon ionization and it is reproduced by first-order perturbation theory (black dotted line); the rapid oscillations reflect the shape of the high-energy tail of the laser spectrum.

first five peaks perfectly. In fact, the ponderomotive shift in (12) makes the energy of the five-photon peak drop below zero at the intensity $9 \times 10^{12} \text{ W cm}^{-2}$, which causes the breakdown of the I^N behaviour of the ionization yield at the highest intensities shown in figure 3. In the intermediate intensity range where the ITPE still gives good ionization yields (see figure 3), the ITPE photoelectron spectrum agrees well with the RTPE result at the first peak but the smaller features at higher electron energy are slightly disturbed or even completely obscured. Single-photon ionization at small laser intensities can be described well by first-order time-dependent perturbation theory, which predicts the photoelectron spectrum

$$S(E) = \left| \langle \psi_E | p | \psi(0) \rangle \int_{-\infty}^{\infty} A(t) e^{i(E - I_p)t} dt \right|^2 \quad (13)$$

with the photoelectron energy E and unbound energy eigenstates $|\psi_E\rangle$. At low intensity, the TDSE result starting in the RTPE agrees perfectly with the perturbative result (see figure 4) whereas the ITPE does not give any reasonable result (not shown). This result confirms our interpretation of the low-intensity behaviour of the ionization yield in figure 3 and it shows that the RTPE method allows us to perform simulations with physical results in situations where other methods may fail.

5. Conclusions

While ITP with the split-operator method is easy to implement, it inherently produces eigenstates that are numerically not perfectly stationary even when fully converged. We demonstrate that this non-stationarity causes problems in the simulation of laser-induced ionization at low laser intensities where the physical results are obscured by artifacts from non-stationary initial states. Our solution—calculating eigenstates of the real-time propagator by an iterative power method—provides noise levels as much as 12 orders of magnitude lower than ITP. In our example system we could show a transition from one-photon to five-photon ionization as the laser intensity is increased, a phenomenon that is only visible with the improved initial state.

For more complex problems, e.g. in three dimensions or with a larger number of active particles, computational efficiency is an issue and the relatively slow convergence of the RTP power method is unfavourable, whereas ITP with adaptive step sizes exhibits quick convergence. However, the advantages of both methods can be combined if the result from ITP is used as initial state for the iterative procedure that finds the desired eigenstates of the real-time propagator. Importantly, this method is not much more difficult to implement than the usual imaginary-time method and thus it has become our weapon of choice when working with the split-operator propagator.

Acknowledgments

The authors acknowledge funding by the Deutsche Forschungsgemeinschaft (DFG) in the frame of the Schwerpunktprogramm (SPP) 1840, Quantum Dynamics in Tailored Intense Fields. We thank S Brennecke for fruitful discussions.

Data availability statement

The data that support the findings of this study are available upon reasonable request from the authors.

ORCID iDs

F Oppermann  <https://orcid.org/0000-0001-7496-1603>
M Lein  <https://orcid.org/0000-0003-1489-8715>

References

- [1] Kosloff R and Tal-Ezer H 1986 *Chem. Phys. Lett.* **127** 223–30
- [2] Bauer D (ed) 2017 *Computational Strong-Field Quantum Dynamics: Intense Light–Matter Interactions* (Berlin: de Gruyter & Co)
- [3] Flamant C, Kolesov G, Manousakis E and Kaxiras E 2019 *J. Chem. Theory Comput.* **15** 6036–45
- [4] Castro A, Marques M A L and Rubio A 2004 *J. Chem. Phys.* **121** 3425–33

- [5] Lode A U J, Sakmann K, Alon O E, Cederbaum L S and Streltsov A I 2012 *Phys. Rev. A* **86** 063606
- [6] Chomaz L *et al* 2018 *Nat. Phys.* **14** 442–6
- [7] Feit M D, Fleck J A and Steiger A 1982 *J. Comput. Phys.* **47** 412–33
- [8] Strang G 1968 *SIAM J. Numer. Anal.* **5** 506–17
- [9] Braun M, Meier C and Engel V 1996 *Comput. Phys. Commun.* **93** 152–8
- [10] Crank J and Nicolson P 1947 *Math. Proc. Camb. Phil. Soc.* **43** 50–67
- [11] Tal-Ezer H and Kosloff R 1984 *J. Chem. Phys.* **81** 3967–71
- [12] Eicke N T 2020 Momentum distributions from bichromatic ionization of atoms and molecules *PhD Thesis* Gottfried Wilhelm Leibniz Universität (Hannover)
- [13] Mises R V and Pollaczek-Geiringer H 1929 *Z. Angew. Math. Mech.* **9** 152–64
- [14] Liu W-C and Clark C W 1992 *J. Phys. B: At. Mol. Opt. Phys.* **25** L517–24
- [15] Bucksbaum P H, Van Woerkom L D, Freeman R R and Schumacher D W 1990 *Phys. Rev. A* **41** 4119–22